# Shuttling an Electron Spin through a Silicon Quantum Dot Array

A.M.J. Zwerver,[1] S.V. Amitonov,[2] S.L. de Snoo,[1] M.T. Mądzik,[1] M. Rimbach-Russ,[1] A. Sammak,[2] G. Scappucci,[1] and L.M.K. Vandersypen[1,*]

[1] *QuTech and Kavli Institute of Nanoscience, Delft University of Technology, Lorentzweg 1, 2628 CJ Delft, Netherlands*

[2] *QuTech and Netherlands Organization for Applied Scientific Research (TNO), Stieltjesweg 1, 2628 CK Delft, Netherlands*

(Received 20 October 2022; revised 22 March 2023; accepted 8 June 2023; published 7 July 2023)

Coherent links between qubits separated by tens of micrometers are expected to facilitate scalable quantum computing architectures for spin qubits in electrically defined quantum dots. These links create space for classical on-chip control electronics between qubit arrays, which can help to alleviate the so-called wiring bottleneck. A promising method of achieving coherent links between distant spin qubits consists of shuttling the spin through an array of quantum dots. Here, we use a linear array of four tunnel-coupled quantum dots in a $^{28}$Si/SiGe heterostructure to create a short quantum link. We move an electron spin through the quantum dot array by adjusting the electrochemical potential for each quantum dot sequentially. By pulsing the gates repeatedly, we shuttle an electron forward and backward through the array up to 250 times, which corresponds to a total distance of approximately 80 μm. We make an estimate of the spin-flip probability per hop in these experiments and conclude that this is well below 0.01% per hop.

DOI: 10.1103/PRXQuantum.4.030303

## I. INTRODUCTION

Practical quantum computation requires millions of high-quality qubits [1]. In light of this, spin qubits in electrically defined quantum dots are of particular interest because they combine a high quality with a small footprint (100-nm pitch) [2]. Recently, long-lived spin coherence [3], high-fidelity single-qubit gates [4–6] and high-fidelity two-qubit gates [7–9] have all been demonstrated, as well as universal control of up to six qubits [10,11]. Moreover, a high fabrication yield can be achieved by employing semiconductor manufacturing techniques [12,13].

It is commonly recognized that for spin qubits, long-range on-chip qubit connections are a crucial part of future devices containing millions of qubits [2,14–17]. The underlying reason is that in current implementations, at least one control wire is routed from off-chip electronics to every qubit on the chip, an approach that becomes impractical beyond thousands or tens of thousands of qubits [18]. To scale beyond, the control signals can be delivered to the chip through a fixed number of wires and distributed to the qubits by classical on-chip electronics. On-chip quantum links would allow us to create space between qubit registers, say, on the 10-μm scale needed for these classical electronics.

Several approaches for on-chip quantum links between spin qubit registers have been proposed and explored. In one approach, qubit information is transferred along a qubit chain via coherent SWAP operations [19,20]. Alternatively, spin qubits could be coherently coupled at a distance by means of microwave photons in superconducting resonators [21–26]. The footprint of the superconducting resonator makes this approach particularly interesting for qubit coupling beyond the 100-μm scale. In a third approach, quantum information transfer is achieved by physically displacing the electrons while preserving the spin state. This has been realized in GaAs by means of surface acoustic waves along up to 20-μm-long channels [27–30]. This method makes use of the piezoelectric effect in GaAs, which is absent in Si.

Electron shuttling propagated by gate voltages offers a promising alternative for spin transfer in silicon on the sub-millimeter scale. The most resource-efficient approach is the so-called conveyor-belt method, where just four phase-shifted sine-wave signals must be applied to a large number of gates to generate a traveling-wave potential along a channel between qubit registers [31]. This conveyor-belt method requires a high degree of uniformity in the channel but has recently been demonstrated in slow motion

*Corresponding author. l.m.k.vandersypen@tudelft.nl

[32]. Bucket-brigade-mode shuttling, where an electron is transported through an array of quantum dots by successively adjusting their electrochemical potentials, offers a more accessible means of exploring spin shuttling, since local potential variations from background disorder can be compensated by individual gate voltages. This method has been successfully demonstrated in GaAs devices, both in linear quantum dot arrays [33,34] and in triangular [35] and two-dimensional arrays [36]. Yet, with the focus of the research field shifting to group-IV platforms due to their superior coherence times because of spin-free isotopes, it is important to demonstrate shuttling in silicon devices. Coherent spin shuttling in silicon poses several new challenges [31,37]. Silicon samples inherently exhibit more electrostatic disorder than GaAs samples, which can hinder the success of the shuttling. Moreover, Si has an extra degree of freedom in the form of the valley [38], which adds an additional loss channel for the moving spin [39]. Promising results have been obtained by shuttling electrons through a linear array of nine Si/SiGe quantum dots with the bucket-brigade mode but without probing the impact on the spin states [40]. So far, coherent spin shuttling in silicon devices has been limited to double-dot experiments [41,42] and spin shuttling through extended quantum dot arrays remains to be demonstrated.

Here, we shuttle a single electron spin through a five-quantum-dot linear array, occupying three or four quantum dots. We move the electron forth and back through the array for up to 1000 hops, equal to a distance of 80 μm, and test both whether the charges are transferred as expected and whether the spin polarization is preserved.

## II. DEVICE AND SHUTTLING PROCEDURE

The quantum dot array [see Fig. 1(a)] is fabricated on an undoped $^{28}$Si/SiGe heterostructure, with the quantum well positioned $\simeq$ 30 nm below the surface (see Appendix A). The device contains three layers of Ti:Pd gate electrodes—used, respectively, as screening gates, plunger and accumulation gates, and barrier gates—isolated by $Al_2O_3$ dielectric layers in between. The device can host a linear array of up to five quantum dots with an 80-nm pitch. The dots are formed by applying a bias to the metallic gate electrodes, where the plunger gates allow for adjustment of the electrochemical potentials of the quantum dots and the barrier gates control the tunnel couplings between the quantum dots. The screening gates define the lateral boundary of the quantum dot array. On either side of the array, a sensing dot is formed, which doubles as electron reservoir. Unless otherwise noted, all charge-sensing data plots show the response of the left-hand sensing dot. All measurements are performed in a dilution refrigerator with a base temperature below 20 mK and with an applied in-plane magnetic field $B_0$ of 1.3 T. This magnetic field gives a Zeeman splitting of 150 μeV, well above the valley splittings in the quantum dots, which are about 80–86 μeV (see Ref. [43, Figs. S5(a)–(c)]).

By means of virtual plunger gates (VP), we tune the five-quantum-dot linear array to the single-electron regime [40,44]. All quantum dots can be formed simultaneously, yet a defect in one of the high-frequency lines connected to the sample prohibits fast control of the fifth quantum dot. As these fast pulses are essential for shuttling, we focus on the leftmost four quantum dots for the remainder of this work. We shuttle over both three quantum dots and four quantum dots [for the charge-stability diagrams, see Figs. 1(b)–1(d)]. The tunnel coupling between the quantum dots is tuned in the range of approximately 4–9 GHz (Appendix F).

A schematic of the shuttling sequence over three quantum dots is depicted in Figs. 1(e) and 1(f). The shuttling procedure starts in the (0, 0, 0) regime, with the three electrochemical potentials of the quantum dots well above the Fermi energy of the reservoir. By pulsing the electrochemical potential of quantum dot 1 deep into the (1,0,0) regime, we load an electron with random spin polarization in quantum dot 1. Then, we sequentially shuttle the electron through the 1–2 anticrossing into the (0,1,0) regime and through the 2–3 anticrossing into (0,0,1). By reversing the sequence, we shuttle the spin back to quantum dot 1.

We repeat the shuttling sequence up to $n$ rounds, ending with the electron in dot 1, and then determine the spin polarization by means of energy-selective readout [45]. The shuttling procedure through four quantum dots is similar, with the addition of a fourth quantum dot. To ensure a well-controlled transition between the quantum dots, we aim to move the electrons through the anticrossings adiabatically with respect to the interdot tunnel coupling. To this effect, we first abruptly pulse to a point close to but before the anticrossing, then ramp through the anticrossing (linear ramp of 2 μs over an approximately 300-μeV detuning range, depending on the dot pair) before we abruptly pulse far beyond the anticrossing. The electrochemical potentials of the quantum dots that are meant to be unoccupied are pulsed well above the Fermi energy of the reservoir, to prevent the electron from tunneling back and to prevent a second electron from entering the array. Shuttling the electron back and forth through multiple dots over multiple rounds mimics shuttling through an extended quantum link and is used to test how well the spin polarization is preserved.

## III. SPIN SHUTTLING

We first verify whether shuttling the electron charge, disregarding the spin state, can be achieved reliably in this sample. To this end, we monitor the (virtual) sensor response while applying a sequence of pulses designed to shuttle the electron through the first three dots for 78 rounds (typical pulse amplitudes are 10–30 mV in

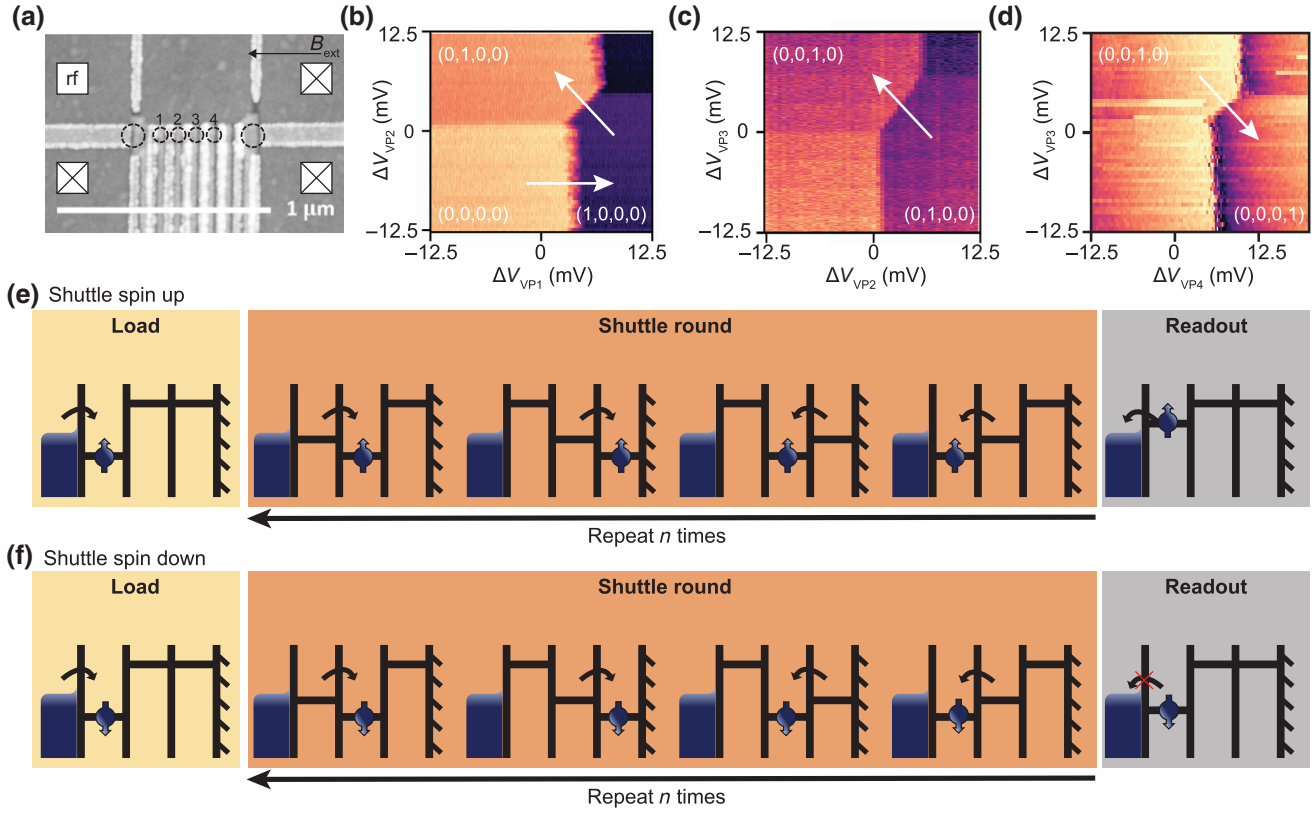


FIG. 1. Shuttling through a Si/SiGe device. (a) A scanning-electron microscope image of a device nominally identical to the device used for this work. The plunger and barrier gates are interleaved and have been fabricated in separate steps. The quantum dots used in this work are indicated by the small circles. The sensing dots on either side of the array are indicated by the large circles. The left-hand sensor is connected to an rf readout circuit via one of the ohmic reservoirs, indicated by squares. This sample does not contain a micromagnet. (b)–(d) Charge-stability diagrams for (b) quantum dots 1–2 while quantum dots 3 and 4 are empty, (c) quantum dots 2–3 while quantum dots 1 and 4 are empty, and (d) quantum dots 4–3 while quantum dots 1 and 2 are empty (right-hand sensing-dot response). The charge-stability diagrams are measured by means of virtual gates. For reference, 25 mV in the virtual gate voltage $\Delta V_{VP1}$ corresponds to 3.75 meV in the electrochemical potential of dot 1. The electron occupation per charge region and the direction of the shuttling events are indicated in the figures. (e),(f) The shuttling procedure through three quantum dots. An electron with random spin is injected during the loading stage: (e) and (f) show the case of a spin up and spin down electron, respectively. At the end of the shuttling sequence, the spin state is read out using energy-selective tunneling, where a spin-up electron will tunnel out of the quantum dot (e), whereas for a spin-down electron this is energetically forbidden (f). The sensing-dot signal reveals whether or not the electron tunneled to the reservoir, from which the spin state is inferred.

virtual gate voltage and 10.5–35.1 mV in real gate voltage). Apart from some latching during the initial electron loading in the array—the tunnel barrier with the reservoir has to be sufficiently closed for the readout protocol to work well—we see the expected sensor response, corresponding to the electron repeatedly occupying the three dots in the sequence 1–2–3–2–1 (Fig. 2). In this data set, the time spent in each dot in between hops is about 420 µs for dots 1 and 3 and half as long for dot 2, such that the total time spent in each dot is the same (Appendix D shows similar data with about 100 µs between hops). The figure shows 100 repetitions of the charge-shuttling experiment, each offset by 0.04 mV in VP1, showing some robustness of the protocol to gate-voltage offsets.

Next, we aim to test to what extent the spin polarization is preserved during shuttling, following a similar procedure as used in earlier spin-shuttling work in a GaAs device [33], shuttling through an array of three and four quantum dots. Given that shuttling through the array over multiple rounds takes time, the spin state will gradually relax to the ground state. The question is whether additional spin flips, beyond those due to spontaneous relaxation, are induced by the act of shuttling itself.

As a reference, we first measure the spin relaxation time in each quantum dot separately. We do so by following the shuttling procedure to move the spin to the desired quantum dot (in this case, using 10-µs ramp times) and varying the wait time in this quantum dot. Thereafter, the electron is shuttled back to quantum dot 1 and its spin state is measured. Repeating this procedure multiple times, we can determine the average spin polarization. For the measurements in quantum dots 2, 3, and

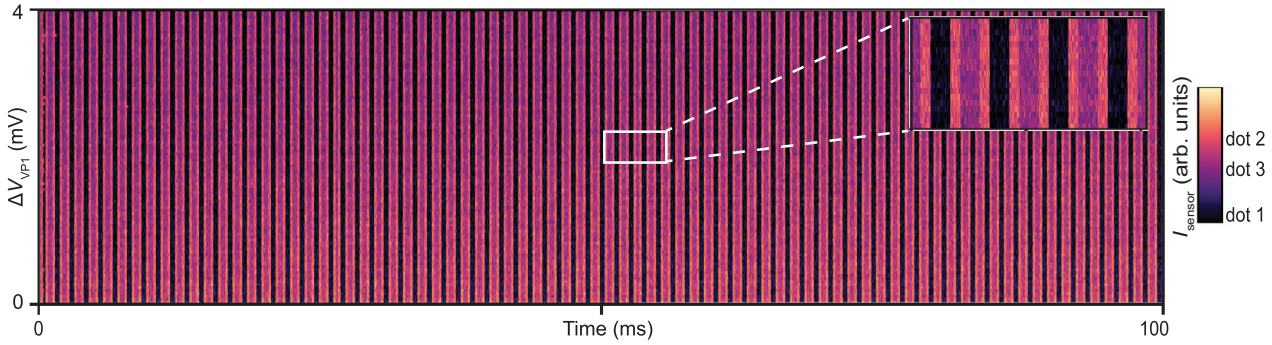


FIG. 2. Charge shuttling over many rounds. The single-shot sensor response for 100 shuttling traces. The spin is loaded in dot 1 and then shuttled forth and back to dot 3 for 78 rounds. Each single-shot trace has an offset with respect to the previous trace of 0.04 mV in $\Delta V_{VP1}$. The inset shows an enlargement of part of the plot to better visualize the sensor response. We see that for each trace, the electron shuttles back and forth repeatedly as expected.

4, the load time in quantum dot 1 is set to 50 μs, to ensure both the loading of an electron in the quantum dot array and potential relaxation to the lower valley [46–49]. We determine relaxation times for quantum dots 1, 2, 3, and 4 of $T_{1,1} = 129 \pm 33$ ms, $T_{1,2} = 257 \pm 79$ ms, $T_{1,3} = 152 \pm 48$ ms, and $T_{1,4} = 145 \pm 71$ ms, respectively, where the uncertainty is one standard deviation (see Appendix E).

Then, we shuttle the electron forth and back through the array once, while the total wait time in the array, $t_{\text{array}}$, is divided symmetrically and equally over the quantum dots. By varying $t_{\text{array}}$, the weighted relaxation time of the spin in the array can be determined. The weighted relaxation time for three dots is plotted in Fig. 3(a), while the weighted relaxation time for shuttling through four dots is plotted in Fig. 3(b) (black circles). Fitting the data to an exponential yields a weighted relaxation time of $T_{1,\text{weighted}} = 170 \pm 18$ ms ($T_{1,\text{weighted}} = 156 \pm 33$ ms) for shuttling through three (four) quantum dots. We expect the weighted $T_1$ to correspond to $3(1/T_{1,1} + 1/T_{1,2} + 1/T_{1,3})^{-1} = 164 \pm 47$ ms ($4(1/T_{1,1} + 1/T_{1,2} + 1/T_{1,3} + 1/T_{1,4})^{-1} = 159 \pm 55$ ms). The measured weighted relaxation time falls within the uncertainty range.

Finally, to analyze the direct effect of shuttling on the spin polarization, we vary both the number of shuttling rounds and the total shuttling time. We load an electron with random spin polarization into the array and shuttle it for a variable number of shuttle rounds through the array for a fixed total duration, $t_{\text{array}}$. Figure 3(a) [Fig. 3(b)] shows the spin-up probability after $n$ shuttling rounds through three (four) dots for $t_{\text{array}}$ varying between 25 ms and 300 ms. Note that each shuttle round through three (four) quantum dots contains four (six) subsequent hops between neighboring quantum dots. For shuttling through three quantum dots, we find that, for each wait time, there

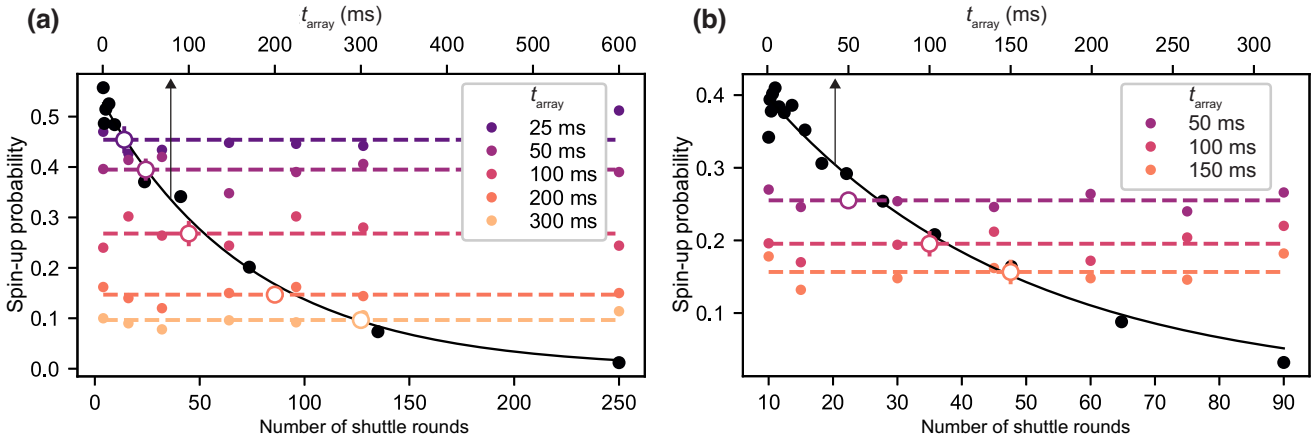


FIG. 3. Shuttling through (a) three and (b) four quantum dots. The colored circles represent the spin-up probability for different times $t_{\text{array}}$ after shuttling the spin back and forth through the array for $n$ rounds (bottom axis). Each data point is averaged 500 times. The dashed colored lines represent the average of the data points for each $t_{\text{array}}$ and are a guide to the eye. This average is also plotted as a function of total time spent in the array (top axis, open circles) with an error bar of one standard deviation (the error bars sometimes fall behind the circles). The black circles show the spin-up probability after shuttling back and forth through the quantum dot array once as a function of the total time spent in the array (top axis). Each data point is averaged (a) 750 and (b) 500 times. Fitting an exponential to the data yields a weighted $T_1$ of (a) $170 \pm 18$ ms and (b) $156 \pm 33$ ms.

is no sign of systematic decay of the spin-up probability as a function of the number of shuttle rounds up to the maximum of $n = 250$ ($n = 500$; see Appendix C) rounds tested. This corresponds to 1000 (2000) hops, or 80 (160) μm of total distance traveled. For shuttling through four quantum dots, the results are analogous up to at least 90 rounds (540 hops and 43 μm). In addition, the average spin-up probability for all shuttling rounds per $t_{\text{array}}$ (shown as the open circles) falls almost exactly on the weighted $T_1$ plot, which further points to the absence of spin flips, other than through spontaneous relaxation during wait times between hops.

The apparent very low spin-flip probability from shuttling is consistent with the observations of Ref. [41] and is also expected considering the known mechanisms for spin flips. Electron exchange with the reservoirs should be suppressed because the dot-reservoir tunnel rate is set to a low value of 32 kHz. Spin flips from hyperfine interaction with nuclear spins should also be negligible in this quantum dot defined in an isotopically enriched $^{28}$Si [800 ppm (parts per million) of $^{29}$Si] quantum well. The spin-orbit interaction is believed to be small in silicon samples, especially in Si/SiGe [38,50], although there are measurements in SiMOS indicating a spin-orbit length of only 1 μm [51]. Finally, we try to obtain a lower bound on the spin-flip probability per hop based on the data of Fig. 3. We analyze the accumulation of errors through transition-induced spin flips by simulating such events and comparing the simulations to the measured data. Even when the probability for transition-induced spin flips is as small as 0.01% per transition, we should see a change in the spin-up probability with the number of shuttle rounds (see Appendix G). This is true irrespective of whether we consider only spin flips from spin up to spin down (a downward trend toward zero spin-up probability with the number of shuttle rounds) or whether we consider equal spin-flip rates in both directions (an upward trend toward 0.5). Finally, fitting the data of Figs. 3(a) and 4 with numerical simulations, we find extremely small spin-flip rates, though with non-negligible uncertainties (see also Appendix G).

The fastest wait times between shuttling used in this experiment amount to about 12.5 μs (500 rounds with four hops per round in a total of 25 ms). This time scale hovers around the $T_2^*$ times measured in isotopically enriched silicon [3,4,7,52–54]. For coherent spin shuttling, the wait times should be reduced by at least one order of magnitude and the shuttling times (2 μs ramp) should also be brought down.

## IV. CONCLUSIONS

In conclusion, we demonstrate the shuttling of an electron through four quantum dots to mimic an array of up to 1000 quantum dots in the bucket-brigade mode, with a spin-flip probability per hop well below 0.01%. The method used in this work can be easily extended to larger quantum dot arrays, which highlights the potential of electron shuttling for long-range quantum links. Subsequent shuttle efforts should focus on decreasing the shuttle time by increasing the tunnel rate between the quantum dots and increasing the ramp rates through the anticrossings, which should all be feasible. In this way, the effect on the qubit coherence of shuttling through extended quantum dot arrays can be studied. In addition, it will be worthwhile to explore high-speed conveyor-belt shuttlers, propagating the electron in a traveling-wave potential [31,32].

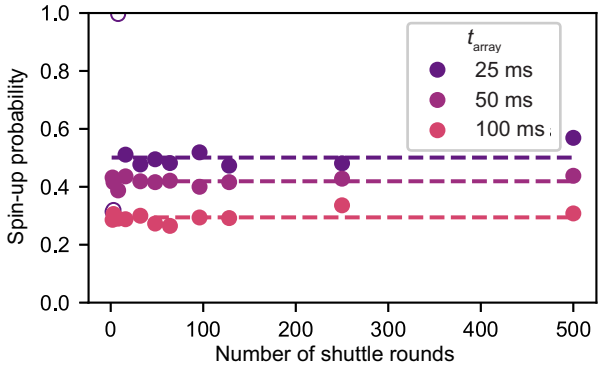


FIG. 4. Shuttling for 500 rounds through an array of three quantum dots (2000 hops). Each data point is the average of 1000 single-shot traces, taken for three different total times in the quantum dot array: 25, 50, and 100 ms. As there is a shift in the readout position during the data collection for the 25-ms case, the first three data points have a calibration error. These outliers are plotted as open circles, yet are not included in further data analysis (see also Fig. 8).

The raw data and analysis that support the findings of this study are available at the Zenodo repository [55].

## ACKNOWLEDGMENTS

We thank Lucas Peters and Zhongyi Jiang for useful input from measuring test structures, Raymond Schouten and Marijn Tiggelman for technical support, and Inga Seidler, Lars Schreiber, Jan Krzywda, and Łukasz Cywiński for useful discussions. Moreover, we thank everyone in the QuTech spin qubit group for input and support. We acknowledge financial support from the QuantERA ERA-NET Cofund in Quantum Technologies, implemented within the European Union Horizon 2020 program and from the Intel Corporation. This research was sponsored by the Army Research Office (ARO) under Grants No. W911NF-17-1-0274 and No. W911NF-12-1-0607. The views and conclusions contained in this document are those of the authors and should not be interpreted as representing the official policies, either expressed or implied, of the ARO or the U.S. Government. The U.S. Government is authorized to reproduce and distribute

reprints for government purposes notwithstanding any copyright notation herein. M.R.R. acknowledges support from the Netherlands Organization of Scientific Research (NWO) under Veni Grant No. VI.Veni.212.223.

## APPENDIX A: DEVICE AND SETUP

The quantum dot array is fabricated on an undoped $^{28}$Si/SiGe heterostructure. The heterostructure contains an 8-nm-strained $^{28}$Si quantum well, with a residual $^{29}$Si concentration of 800 ppm, separated from the surface by a 30-nm-thick $Si_{0.7}$-$Ge_{0.3}$ spacer and a sacrificial 2-nm Si capping layer. The device contains three layers of Ti:Pd metallic gates, used, respectively, as screening gates (3:17 nm), accumulation or plunger gates (3:27 nm), and barrier gates (3:27 nm). The metallic gates are isolated from each other by 5-nm $Al_2$-$O_3$ dielectrics, deposited using atomic layer deposition. Further details of the device fabrication methods and sample screening can be found in Refs. [56] and [11], respectively.

The measurements are carried out in an Oxford Triton dry dilution refrigerator with a base temperature around 10 mK. The dc part of the setup consists of two in-house-built battery-powered voltage sources, containing digital-to-analog converters. The voltage pulses applied to the sample are generated by two Tektronix AWG5014 arbitrary wave form generators and sent to the sample via coaxial lines, connected via a bias tee on the printed circuit board with a cutoff frequency of 3 Hz. The response of the left-hand charge sensor is monitored with an rf-reflectometry setup at a resonance frequency of $f = 214$ MHz, containing an in-house-fabricated Nb-Ti-N inductor. The reflectometry signal is amplified at the 4-K plate and demodulated using an in-house-built demodulation setup. The sensor response of the right-hand charge sensor is converted to voltage through a home-built baseband amplifier. The latter signal is not used for single-shot readout.

## APPENDIX B: DATA PROCESSING OF TIME TRACES

To analyze the spin state after shuttling, we smoothen the data of the time traces by means of boxcar averaging; we average each data point with the 25 points around it. Subsequently, we assign each time trace "0" or "1" by means of relative thresholding (adjusting the threshold based on the signal of a readout segment during which the first dot is always occupied with one electron). During the measurements, we encounter a timing problem between the AWG and the digitizer, which results in an offset of up to 50 μs in the time traces for different shuttle rounds (see Fig. 8). To ensure a similar readout duration for each trace, we cut off the start and end of each time trace by the same number of points.

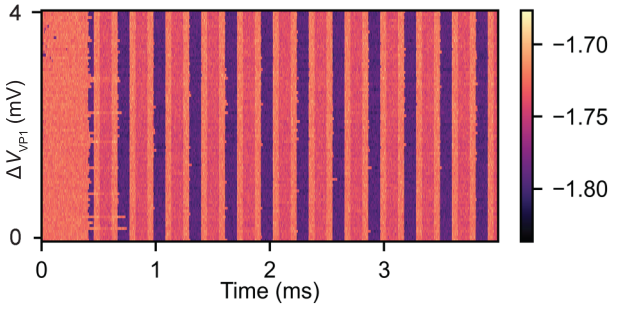


FIG. 5. Charge-shuttling data showing the approximately 11 first shuttling rounds of a shuttling sequence of 78 rounds, showing the sensor response for 100 repetitions (each trace has an offset with respect to the previous trace of 0.04 mV in $\Delta V_{VP1}$). The time between hops is about 100 μs for dots 1 and 3 (50 μs for dot 2), roughly 4 times shorter compared to the data in Fig. 2. By examining an enlargement of the first 11 shuttling rounds, latching effects during loading from the reservoir can be seen in a subset of the traces. Even during the shuttling rounds, it can be seen that in some cases the electron passes from one dot to the next with a small delay. We observe that this jitter only occurs while shuttling from dot 1 to dot 2 and is not symmetric. Moreover, the jitter in this figure is on average 7 μs long, while this jitter does not appear in other transitions that we monitor, where the electron spends only 10 μs per quantum dot. While we do not understand the origin of the small delay in electron transfer for the transition from dot 1 to dot 2, such small delays are not a generic limitation of this type of device. Earlier work on devices with similar geometries has also demonstrated fast and controlled transfer of electrons through quantum dot arrays [40], as will be necessary for phase coherent spin shuttling in future experiments.

## APPENDIX C: SHUTTLING FOR 500 ROUNDS

The data for shuttling through three quantum dots for up to 500 shuttling rounds are shown in Fig. 4.

## APPENDIX D: CHARGE SHUTTLING OVER MANY ROUNDS

Figure 5 shows charge-sensing data where a charge is shuttled through the array of three quantum dots many times, 4 times faster than in Fig. 2.

## APPENDIX E: RELAXATION TIMES IN EACH QUANTUM DOT

Figure 6 shows the data from which the spin relaxation times are extracted for each dot separately.

## APPENDIX F: TUNNEL COUPLING

Measurements of the tunnel coupling between the subsequent quantum dots are shown in Fig. 7. The data are fitted with the model from Refs. [57,58], where the tunnel-coupling gap is defined as $2t_c$, so the tunnel coupling is taken as the half gap. The tunnel coupling extracted from

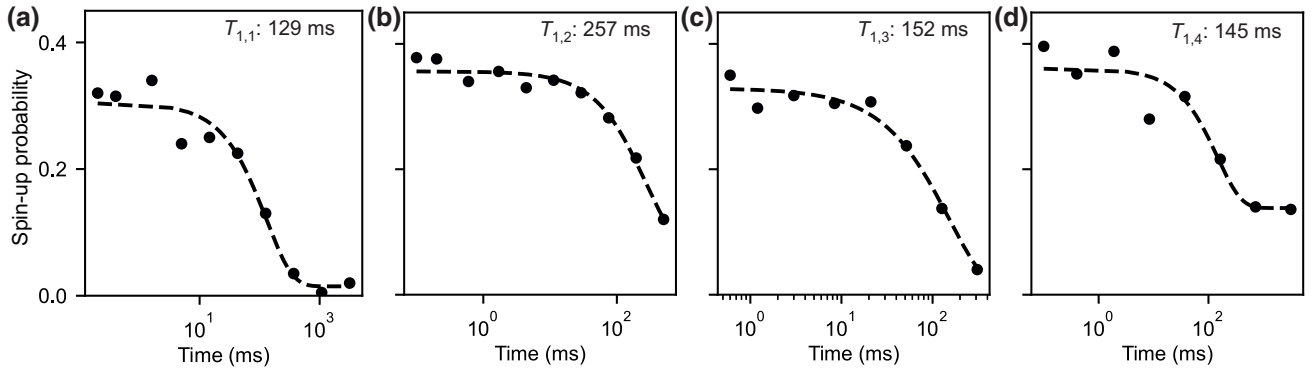


FIG. 6. Relaxation times for the separate quantum dots. The spin-up probability of a randomly loaded spin as a function of the waiting time in (a) dot 1, (b) dot 2, (c) dot 3, and (d) dot 4 at a magnetic field of 1.3 T. Each data point is averaged 300, 500, 400, and 250 times for dots 1, 2, 3, and 4, respectively. Fitting the data to an exponential decay yields relaxation times of $T_{1,1} = 129 \pm 33$ ms, $T_{1,2} = 257 \pm 79$ ms, $T_{1,3} = 152 \pm 48$ ms, and $T_{1,4} = 145 \pm 71$ ms. The relatively large error bars are a result of the sparsity of data points for longer waiting times.

the fit for each interdot transition is given in microelectronvolts. The lever arm of $P_5$ to dot 5 is extracted from Coulomb diamonds. The lever arms of the virtual plunger gates to the respective dot potentials are successively determined from charge-stability diagrams (by comparing the relative capacitive coupling of each virtual gate to that of gates with previously extracted lever arms). For the fit, we use an electron temperature of 75 mK, which is similar to what has been measured in previous and later cooldowns. The signal-to-noise ratio for the 2–3 interdot transition is relatively low, because of the distance to the sensing dot and the sensing-dot sensitivity.

## APPENDIX G: SIMULATION OF SPIN-FLIP ERRORS FROM SHUTTLING

We aim to bound the spin-flip probability per hop by comparing the experimental data with numerical simulations. In our simulations, we consider spin relaxation from spin up to spin down and a finite spin-flip probability per hopping event that is either the same for upward or downward spin flips [Fig. 9(a)] or assumes that spin flips occur only from spin up to spin down [Fig. 9(d)]. Since the time between events is expected to be on the order of $T_2^*$ or larger, we neglect the phase evolution in our simulations and restrict ourselves to the dynamics of the spin-up and spin-down probabilities $P_{|\uparrow\rangle}$ and $P_{|\downarrow\rangle}$. In this model, relaxation for quantum dot $j$ reads, in the basis $\{|\uparrow\rangle,|\downarrow\rangle\}$,

$$R_j = \begin{pmatrix} \exp[-t_{\mathrm{wait}}/T_{1,j}] & 0 \\ 1-\exp[-t_{\mathrm{wait}}/T_{1,j}] & 1 \end{pmatrix}. \tag{G1}$$

The spin-flip probability matrix, with spin-flip probability $\beta$, is

$$F = \begin{pmatrix} 1-\beta & \beta \\ \beta & 1-\beta \end{pmatrix}, \tag{G2}$$

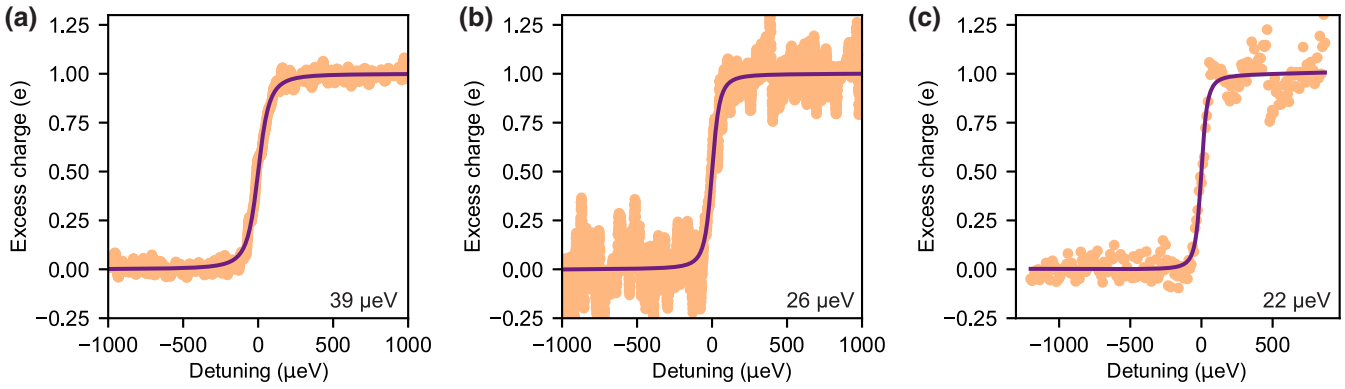


FIG. 7. Tunnel coupling. Excess charge (in units of e) as a function of detuning at the interdot transitions of (a) dots 1 and 2 (1,0,0,0)-(0,1,0,0), (b) dots 2 and 3 (0,1,0,0)-(0,0,1,0) and (c) dots 3 and 4 (0,0,1,0)-(0,0,0,1), measured with the right-hand sensing dot. The extracted tunnel couplings are presented in microelectronvolt.

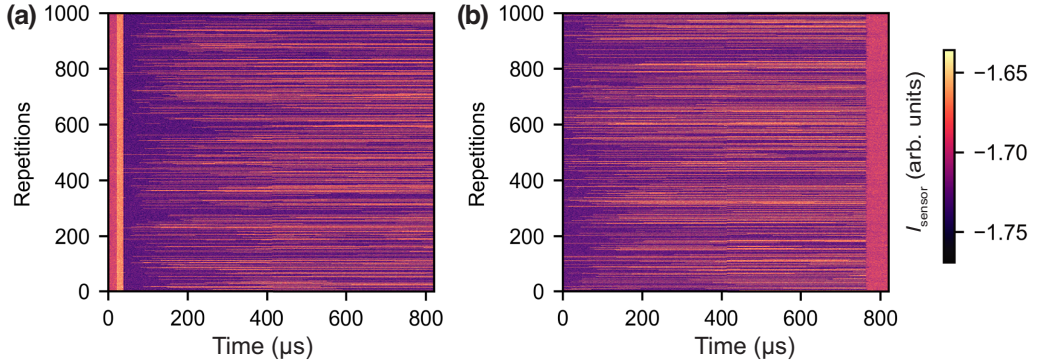


FIG. 8. Single-shot traces for two different data points in Fig. 4. Single-shot traces showing the sensing-dot response of the readout segment after shuttling the electron (a) 500 and (b) 250 rounds through the array, respectively, for $t_{\mathrm{array}} = 50$ ms. The pink lines indicate a blip, meaning that a tunneling event has happened (spin up). A purple line indicates the absence of a blip and thus represents a spin-down electron. (a) The digitizer timing is slightly offset with respect to the readout pulse; the last two shuttling steps are still visible on the left-hand side of each trace. (b) The digitizer timing is offset with respect to the readout pulse; the start of the compensation pulse is seen on the right-hand side of each trace.

for symmetric spin flips. When we consider spin flips from spin up to spin down only, the matrix becomes

$$F = \begin{pmatrix} 1-\beta & 0 \\ \beta & 1 \end{pmatrix}, \tag{G3}$$

The time spent in each quantum dot depends on the total time in the array, $t_{\mathrm{array}}$, and the number of shuttle rounds $n$ as $t_{\mathrm{wait}} = t_{\mathrm{array}}/(6n)$, where the factor of 6 accounts for the six stages of the shuttling sequence (1–2–3–3–2–1). After

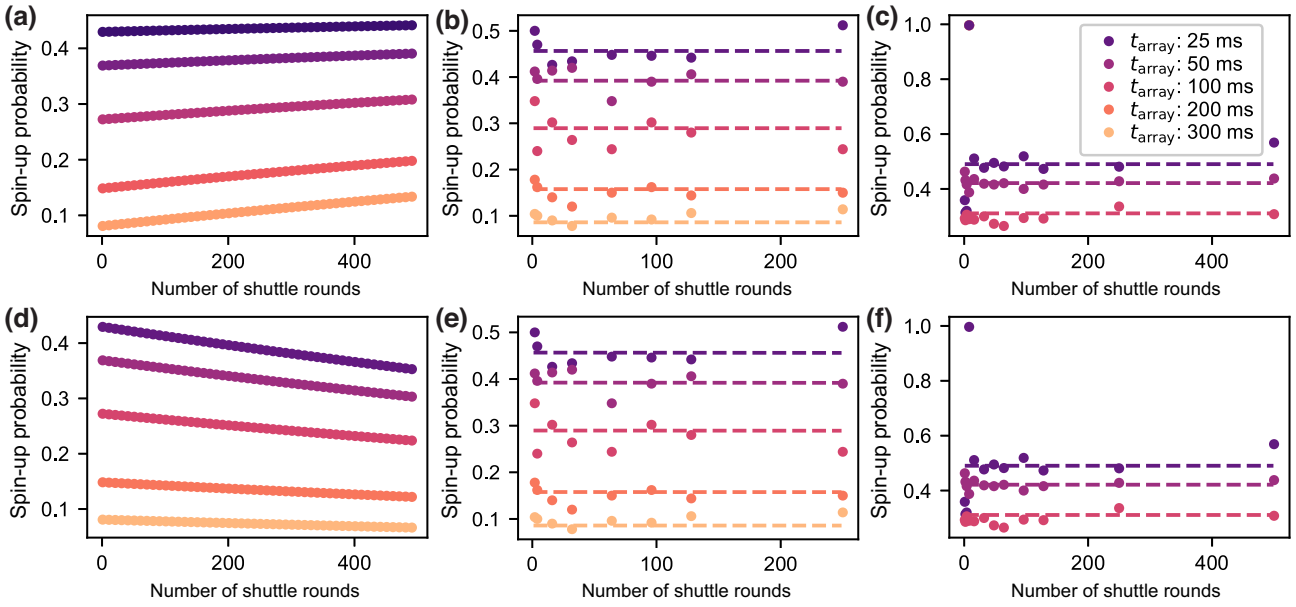


FIG. 9. The simulation and fitting of possible spin-flip models. (a),(d) Simulation of the spin-up probability at the end of a shuttling sequence through three dots for (a) symmetric spin flips and (d) asymmetric spin flips, considering in both cases a 0.01% probability of a spin flip per hop and $T_1$ decay during the wait times in the dots, for different $t_{\mathrm{array}}$. (b),(c) The fit of the numerical spin-flip model considering a symmetric spin flip to the shuttle data of shuttling (b) 250 rounds and (c) 500 rounds through three quantum dots. (e),(f) The fit of the numerical spin-flip model considering an asymmetric spin flip to the shuttle data of shuttling (e) 250 rounds and (f) 500 rounds through three quantum dots. For all four panels, the fit parameters are the spin-flip probability and the initial spin-up probability. These two parameters are fitted simultaneously for all five (three) values of $t_{\mathrm{array}}$ in a panel. The fit parameters per panel are as follows: (b) initial spin-up probability $53.1 \pm 0.8\%$, symmetric spin-flip probability per hop $0.00 \pm 0.005\%$; (c) initial spin-up probability $56.9 \pm 0.6\%$, symmetric spin-flip probability per hop $0.00 \pm 0.008\%$; (e) initial spin-up probability $53.2 \pm 1\%$, asymmetric spin-flip probability per hop $0.00 \pm 0.004\%$, (f) initial spin-up probability $56.9 \pm 0.8\%$, asymmetric spin-flip probability per hop $0.00 \pm 0.002\%$. In all cases, the error bars are one standard deviation around the mean. Given that both the symmetric and asymmetric model fit the data very well, the fit quality in itself does not allow us to conclude that one model captures the physics better than the other.

$n$ shuttle rounds, the final spin probabilities are as follows:

$$\begin{pmatrix} P_{|\uparrow\rangle,\text{final}} \\ P_{|\downarrow\rangle,\text{final}} \end{pmatrix} = (R_1 F R_2 F R_3 R_3 F R_2 F R_1)^n \begin{pmatrix} P_{|\uparrow\rangle,\text{init}} \\ P_{|\downarrow\rangle,\text{init}} \end{pmatrix}. \quad \text{(G4)}$$

Figure 9(a) [(d)] shows numerical-simulation results considering a symmetric (asymmetric) spin-flip probability per hop of 0.01%, spin relaxation during the wait times between hops, with time constants $T_{1,1}$, $T_{1,2}$, and $T_{1,3}$, as measured in Fig. 6, and initial probabilities $P_{|\uparrow\rangle,\text{init}} = P_{|\uparrow\rangle,\text{init}} = 0.5$. The simulation shows the resulting spin-up probability as a function of the number of shuttle rounds $n$. Especially for the longer array times, the spin-up probability follows an unmistakable upward (downward) trend with the number of shuttle rounds. In contrast, no upward or downward trend can be seen in the experiment of Fig. 3, indicating that the experimental spin-flip probability per hop is well below 0.01%.

We then proceed by fitting this numerical model to the shuttle data of Fig. 3(a) (250 rounds of shuttling through three dots) and Fig. 4 (500 rounds of shuttling through three dots), where the fit parameters are the initial spin up probability and the spin-flip probability. As the spin-flip probability should not change for different $t_{\text{array}}$, we fit all the data per panel to the same initial spin up probability and spin-flip probability. We fit models for both symmetric spin flips [see Figs. 9(c) and 9(d)] and asymmetric spin flips [see Figs. 9(e) and 9(f)]. For all four fits, we find extremely small spin-flip probabilities, though with non-negligible uncertainties. The spin-flip probability for 500 shuttle rounds is typically smaller than the spin-flip probability for 250 shuttle rounds, because of the extra shuttle rounds taken into account. The initial spin-flip probabilities for the symmetric and asymmetric flip fits are practically similar, which indicates some robustness of this fit parameter.


[1] M. Reihera, N. Wiebeb, K. Svoreb, D. Weckerb, and M. Troyer, Elucidating reaction mechanisms on quantum computers, Proc. Natl. Acad. Sci. **114**, 7555 (2017).

[2] L. M. K. Vandersypen, H. Bluhm, J. S. Clarke, A. S. Dzurak, R. Ishihara, A. Morello, D. J. Reilly, L. R. Schreiber, and M. Veldhorst, Interfacing spin qubits in quantum dots and donors—hot, dense, and coherent, npj Quantum Inf. **3**, 34 (2017).

[3] M. Veldhorst, J. C. C. Hwang, C. H. Yang, A. W. Leenstra, B. de Ronde, J. P. Dehollain, J. T. Muhonen, F. E. Hudson, K. M. Itoh, A. Morello, and A. S. Dzurak, An addressable quantum dot qubit with fault-tolerant control-fidelity, Nat. Nanotechnol. **9**, 981 (2014).

[4] J. Yoneda, K. Takeda, T. Otsuka, T. Nakajima, M. R. Delbecq, G. Allison, T. Honda, T. Kodera, S. Oda, Y. Hoshi, N. Usami, K. M. Itoh, and S. Tarucha, A quantum-dot spin qubit with coherence limited by charge noise and fidelity higher than 99.9%, Nat. Nanotechnol. **13**, 102 (2018).

[5] C. H. Yang, K. W. Chan, R. Harper, W. Huang, T. Evans, J. C. C. Hwang, B. Hensen, A. Laucht, T. Tanttu, F. E. Hudson, S. T. Flammia, K. M. Itoh, A. Morello, S. D. Bartlett, and A. S. Dzurak, Silicon qubit fidelities approaching incoherent noise limits via pulse engineering, Nat. Electron. **2**, 151 (2019).

[6] W. I. L. Lawrie, M. Russ, F. van Riggelen, N. W. Hendrickx, S. L. de Snoo, A. Sammak, G. Scappucci, and M. Veldhorst, Simultaneous driving of semiconductor spin qubits at the fault-tolerant threshold, Nat. Comm. **14**, 3617 (2023).

[7] X. Xue, M. Russ, N. Samkharadze, B. Undseth, A. Sammak, G. Scappucci, and L. M. K. Vandersypen, Quantum logic with spin qubits crossing the surface code threshold, Nature **601**, 343 (2022).

[8] A. Noiri, K. Takeda, T. Nakajima, T. Kobayashi, A. Sammak, G. Scappucci, and S. Tarucha, Fast universal quantum gate above the fault-tolerance threshold in silicon, Nature **601**, 338 (2022).

[9] A. R. Mills, C. R. Guinn, M. J. Gullans, A. J. Sigillito, M. M. Feldman, E. Nielsen, and J. R. Petta, Two-qubit silicon quantum processor with operation fidelity exceeding 99%, Sci. Adv. **8**, eabn5130 (2022).

[10] N. W. Hendrickx, W. I. L. Lawrie, M. Russ, F. van Riggelen, S. L. de Snoo, R. N. Schouten, A. Sammak, G. Scappucci, and M. Veldhorst, A four-qubit germanium quantum processor, Nature **591**, 580 (2021).

[11] S. G. J. Philips, M. T. Mądzik, S. V. Amitonov, S. L. de Snoo, M. Russ, N. Kalhor, C. Volk, W. I. L. Lawrie, D. Brousse, L. Tryputen, B. P. Wuetz, A. Sammak, M. Veldhorst, G. Scappucci, and L. M. K. Vandersypen, Universal control of a six-qubit quantum processor in silicon, Nature **609**, 919 (2022).

[12] R. Maurand, X. Jehl, D. Kotekar-Patil, A. Corna, H. Bohuslavskyi, R. Laviéville, L. Hutin, S. Barraud, M. Vinet, M. Sanquer, and S. De Franceschi, A CMOS silicon spin qubit, Nat. Commun. **7**, 13575 (2016).

[13] A. M. J. Zwerver *et al.*, Qubits made by advanced semiconductor manufacturing, Nat. Electron. **5**, 184 (2022).

[14] J. M. Taylor, H.-A. Engel, W. Dür, A. Yacoby, C. M. Marcus, P. Zoller, and M. D. Lukin, Fault-tolerant architecture for quantum computation using electrically controlled semiconductor spins, Nat. Phys. **1**, 177 (2005).

[15] R. Li, L. Petit, D. P. Franke, J. P. Dehollain, J. Helsen, M. Steudtner, N. K. Thomas, Z. R. Yoscovits, K. J. Singh, S. Wehner, L. M. K. Vandersypen, J. S. Clarke, and M. Veldhorst, A crossbar network for silicon quantum dot qubits, Sci. Adv. **4**, eaar3960 (2018).

[16] B. Buonacorsi, Z. Cai, E. B. Ramirez, K. S. Willick, S. M. Walker, J. Li, B. D. Shaw, X. Xu, S. C. Benjamin, and J. Baugh, Network architecture for a topological quantum computer in silicon, Quantum Sci. Technol. **4**, 025003 (2019).

[17] J. M. Boter, J. P. Dehollain, J. P. G. van Dijk, Y. Xu, T. Hensgens, R. Versluis, H. W. L. Naus, J. S. Clarke, M. Veldhorst, F. Sebastiano, and L. M. K. Vandersypen, The Spider-Web Array—a Sparse Spin Qubit Array, Phys. Rev. Appl. **18**, 024053 (2022).

[18] D. Franke, J. Clarke, L. Vandersypen, and M. Veldhorst, Rent's rule and extensibility in quantum computing, Microprocess. Microsyst. **67**, 1 (2019).

[19] M. Friesen, A. Biswas, X. Hu, and D. Lidar, Efficient Multiqubit Entanglement via a Spin Bus, Phys. Rev. Lett. **98**, 230503 (2007).

[20] Y. P. Kandel, H. Qiao, S. Fallahi, G. C. Gardner, M. J. Manfra, and J. M. Nichol, Coherent spin-state transfer via Heisenberg exchange, Nature **573**, 553 (2019).

[21] S. P. Harvey, C. G. L. Bøttcher, L. A. Orona, S. D. Bartlett, A. C. Doherty, and A. Yacoby, Coupling two spin qubits with a high-impedance resonator, Phys. Rev. B **97**, 235409 (2018).

[22] X. Mi, M. Benito, S. Putz, D. M. Zajac, J. M. Taylor, G. Burkard, and J. R. Petta, A coherent spin-photon interface in silicon, Nature **555**, 599 (2018).

[23] N. Samkharadze, G. Zheng, N. Kalhor, D. Brousse, A. Sammak, U. C. Mendes, A. Blais, G. Scappucci, and L. M. K. Vandersypen, Strong spin-photon coupling in silicon, Science **359**, 1123 (2018).

[24] A. J. Landig, J. V. Koski, P. Scarlino, U. C. Mendes, A. Blais, C. Reichl, W. Wegscheider, A. Wallraff, K. Ensslin, and T. Ihn, Coherent spin-photon coupling using a resonant exchange qubit, Nature **560**, 179 (2018).

[25] F. Borjans, X. G. Croot, X. Mi, M. J. Gullans, and J. R. Petta, Resonant microwave-mediated interactions between distant electron spins, Nature **577**, 195 (2020).

[26] P. Harvey-Collard, J. Dijkema, G. Zheng, A. Sammak, G. Scappucci, and L. M. K. Vandersypen, Coherent Spin-Spin Coupling Mediated by Virtual Microwave Photons, Phys. Rev. X **12**, 021026 (2022).

[27] R. P. G. McNeil, M. Kataoka, C. J. B. Ford, C. H. W. Barnes, D. Anderson, G. A. C. Jones, I. Farrer, and D. A. Ritchie, On-demand single-electron transfer between distant quantum dots, Nature **477**, 439 (2011).

[28] S. Hermelin, S. Takada, M. Yamamoto, S. Tarucha, A. D. Wieck, L. Saminadayar, C. Bäuerle, and T. Meunier, Electrons surfing on a sound wave as a platform for quantum optics with flying electrons, Nature **477**, 435 (2011).

[29] B. Jadot, P.-A. Mortemousque, E. Chanrion, V. Thiney, A. Ludwig, A. D. Wieck, M. Urdampilleta, C. Bäuerle, and T. Meunier, Distant spin entanglement via fast and coherent electron shuttling, Nat. Nanotechnol. **16**, 570 (2021).

[30] H. Edlbauer, J. Wang, S. Ota, A. Richard, B. Jadot, P.-A. Mortemousque, Y. Okazaki, S. Nakamura, T. Kodera, N.-H. Kaneko, A. Ludwig, A. D. Wieck, M. Urdampilleta, T. Meunier, C. Bäuerle, and S. Takada, In-flight distribution of an electron within a surface acoustic wave, Appl. Phys. Lett. **119**, 114004 (2021).

[31] V. Langrock, J. A. Krzywda, N. Focke, I. Seidler, L. R. Schreiber, and Ł. Cywiński, Blueprint of a Scalable Spin Qubit Shuttle Device for Coherent Mid-Range Qubit Transfer in Disordered Si/SiGe/$SiO_2$, PRX Quantum **4**, 020305 (2023).

[32] I. Seidler, T. Struck, R. Xue, N. Focke, S. Trellenkamp, H. Bluhm, and L. R. Schreiber, Conveyor-mode single-electron shuttling in Si/SiGe for a scalable quantum computing architecture, npj Quantum Inf. **8**, 100 (2022).

[33] T. A. Baart, M. Shafiei, T. Fujita, C. Reichl, W. Wegscheider, and L. M. K. Vandersypen, Single-spin CCD, Nat. Nanotechnol. **11**, 330 (2016).

[34] T. Fujita, T. Baart, C. Reichl, W. Wegscheider, and L. Vandersypen, Coherent shuttle of electron-spin states, npj Quantum Inf. **3**, 22 (2017).

[35] H. Flentje, P.-A. Mortemousque, R. Thalineau, A. Ludwig, A. D. Wieck, C. Bäuerle, and T. Meunier, Coherent long-distance displacement of individual electron spins, Nat. Commun. **8**, 501 (2017).

[36] P.-A. Mortemousque, B. Jadot, E. Chanrion, V. Thiney, C. Bäuerle, A. Ludwig, A. D. Wieck, M. Urdampilleta, and T. Meunier, Enhanced Spin Coherence While Displacing Electron in a Two-Dimensional Array of Quantum Dots, PRX Quantum **2**, 030331 (2021).

[37] J. A. Krzywda and Ł. Cywiński, Interplay of charge noise and coupling to phonons in adiabatic electron transfer between quantum dots, Phys. Rev. B **104**, 075439 (2021).

[38] F. A. Zwanenburg, A. S. Dzurak, A. Morello, M. Y. Simmons, L. C. L. Hollenberg, G. Klimeck, S. Rogge, S. N. Coppersmith, and M. A. Eriksson, Silicon quantum electronics, Rev. Mod. Phys. **85**, 961 (2013).

[39] M. Friesen, S. Chutia, C. Tahan, and S. N. Coppersmith, Valley splitting theory of SiGe/Si/SiGe quantum wells, Phys. Rev. B **75**, 115318 (2007).

[40] A. R. Mills, D. M. Zajac, M. J. Gullans, F. J. Schupp, T. M. Hazard, and J. R. Petta, Shuttling a single charge across a one-dimensional array of silicon quantum dots, Nat. Commun. **10**, 1063 (2019).

[41] J. Yoneda, W. Huang, M. Feng, C. H. Yang, K. W. Chan, T. Tanttu, W. Gilbert, R. C. C. Leon, F. E. Hudson, K. M. Itoh, A. Morello, S. D. Bartlett, A. Laucht, A. Saraiva, and A. S. Dzurak, Coherent spin qubit transport in silicon, Nat. Commun. **12**, 4114 (2021).

[42] A. Noiri, K. Takeda, T. Nakajima, T. Kobayashi, A. Sammak, G. Scappucci, and S. Tarucha, A shuttling-based two-qubit logic gate for linking distant silicon quantum processors, Nat. Commun. **13**, 5740 (2022).

[43] B. Paquelet Wuetz, M. P. Losert, S. Koelling, L. E. A. Stehouwer, A.-M. J. Zwerver, S. G. J. Philips, M. T. Mądzik, X. Xue, G. Zheng, M. Lodari, S. V. Amitonov, N. Samkharadze, A. Sammak, L. M. K. Vandersypen, R. Rahman, S. N. Coppersmith, O. Moutanabbir, M. Friesen, and G. Scappucci, Atomic fluctuations lifting the energy degeneracy in Si/SiGe quantum dots, Nat. Commun. **13**, 7730 (2022).

[44] C. Volk, A. M. J. Zwerver, U. Mukhopadhyay, P. T. Eendebak, C. J. van Diepen, J. P. Dehollain, T. Hensgens, T. Fujita, C. Reichl, W. Wegscheider, and L. M. K. Vandersypen, Loading a quantum-dot based "Qubyte" register, npj Quantum Inf. **5**, 29 (2019).

[45] J. M. Elzerman, R. Hanson, L. H. Willems van Beveren, B. Witkamp, L. M. K. Vandersypen, and L. P. Kouwenhoven, Single-shot read-out of an individual electron spin in a quantum dot, Nature **430**, 431 (2004).

[46] C. H. Yang, A. Rossi, R. Ruskov, N. S. Lai, F. A. Mohiyaddin, S. Lee, C. Tahan, G. Klimeck, A. Morello, and A. S. Dzurak, Spin-valley lifetimes in a silicon quantum dot with tunable valley splitting, Nat. Commun. **4**, 2069 (2013).

[47] T. F. Watson, S. G. J. Philips, E. Kawakami, D. R. Ward, P. Scarlino, M. Veldhorst, D. E. Savage, M. G. Lagally, M. Friesen, S. N. Coppersmith, M. A. Eriksson, and L. M. K. Vandersypen, A programmable two-qubit quantum processor in silicon, Nature **555**, 633 (2018).

[48] F. Borjans, D. M. Zajac, T. M. Hazard, and J. R. Petta, Single-Spin Relaxation in a Synthetic Spin-Orbit Field, Phys. Rev. Appl. **11**, 044063 (2019).

[49] X. Cai, E. J. Connors, L. F. Edge, and J. M. Nichol, Coherent spin-valley oscillations in silicon, Nat. Phys. **19**, 386 (2023).

[50] M. Prada, G. Klimeck, and R. Joynt, Spin-orbit splittings in Si/SiGe quantum wells: From ideal Si membranes to realistic heterostructures, New J. Phys. **13**, 013009 (2011).

[51] P. Harvey-Collard, N. T. Jacobson, C. Bureau-Oxton, R. M. Jock, V. Srinivasa, A. M. Mounce, D. R. Ward, J. M. Anderson, R. P. Manginell, J. R. Wendt, T. Pluym, M. P. Lilly, D. R. Luhman, M. Pioro-Ladrière, and M. S. Carroll, Spin-Orbit Interactions for Singlet-Triplet Qubits in Silicon, Phys. Rev. Lett. **122**, 217702 (2019).

[52] A. J. Sigillito, M. J. Gullans, L. F. Edge, M. Borselli, and J. R. Petta, Coherent transfer of quantum information in a silicon double quantum dot using resonant SWAP gates, npj Quantum Inf. **5**, 110 (2019).

[53] W. Huang, C. H. Yang, K. W. Chan, T. Tanttu, B. Hensen, R. C. C. Leon, M. A. Fogarty, J. C. C. Hwang, F. E. Hudson, K. M. Itoh, A. Morello, A. Laucht, and A. S. Dzurak, Fidelity benchmarks for two-qubit gates in silicon, Nature **569**, 532 (2019).

[54] T. Struck, A. Hollmann, F. Schauer, O. Fedorets, A. Schmidbauer, K. Sawano, H. Riemann, N. V. Abrosimov, Ł. Cywiński, D. Bougeard, and L. R. Schreiber, Low-frequency spin qubit energy splitting noise in highly purified $^{28}$Si/SiGe, npj Quantum Inf. **6**, 40 (2020).

[55] https://doi.org/10.5281/zenodo.8088080

[56] W. I. L. Lawrie, H. G. J. Eenink, N. W. Hendrickx, J. M. Boter, L. Petit, S. V. Amitonov, M. Lodari, B. Paquelet Wuetz, C. Volk, S. G. J. Philips, G. Droulers, N. Kalhor, F. van Riggelen, D. Brousse, A. Sammak, L. M. K. Vandersypen, G. Scappucci, and M. Veldhorst, Quantum dot arrays in silicon and germanium, Appl. Phys. Lett. **116**, 080501 (2020).

[57] L. DiCarlo, H. J. Lynch, A. C. Johnson, L. I. Childress, K. Crockett, C. M. Marcus, M. P. Hanson, and A. C. Gossard, Differential Charge Sensing and Charge Delocalization in a Tunable Double Quantum Dot, Phys. Rev. Lett. **92**, 226801 (2004).

[58] C. J. van Diepen, P. T. Eendebak, B. T. Buijtendorp, U. Mukhopadhyay, T. Fujita, C. Reichl, W. Wegscheider, and L. M. K. Vandersypen, Automated tuning of inter-dot tunnel coupling in double quantum dots, Appl. Phys. Lett. **113**, 033101 (2018).